J Mater Sci (2010) 45:3190–3197
DOI 10.1007/s10853-010-4326-6

AFM indentation method used for elastic modulus characterization of interfaces and thin layers

M. A. Monclus · T. J. Young · D. Di Maio

Received: 2 December 2009 / Accepted: 13 February 2010 / Published online: 4 March 2010
© Springer Science+Business Media, LLC 2010

Abstract Atomic force microscopy (AFM) is increasingly being used as a nanoindentation tool to measure local elastic properties of surfaces. In this article, a method based on AFM in force volume (force curve mapping) mode is employed to measure the elastic modulus distribution at the interface of a glass flake-reinforced polypropylene sample and at a lead-free Cu–solder joint. Indentation arrays are performed using a diamond AFM tip. The processing of experimental AFM indentation data is automated by customized software that can analyse and calibrate multiple force curves. The analysis algorithm corrects the obtained force curves by selecting the contact point, discarding the non-contact region and subtracting the cantilever deflection from the measured force curve in order to obtain true indentation curves. A Hertzian model is then applied to the resulting AFM indentation data. Reference materials are used to estimate the tip radius needed to extract the elastic modulus values. With the proposed AFM measurement method, we are able to obtain high-resolution maps showing elastic modulus variations around a composite interface and a Cu–solder joint. No distinct interphase region is detected in the composite case, whereas a separate intermetallic layer (1–2 μm thick) of much higher Young's modulus (~131 GPa) than Cu and solder material is identified in the Cu–solder joint. Elastic modulus results obtained for the Cu (~72 GPa), solder (~50 GPa) and glass (~65 GPa) materials are comparable to the results obtained by instrumented indentation [~73, ~46 and ~61 GPa], which accentuates the potential of this method for applications requiring high lateral resolution.

M. A. Monclus (✉) · D. Di Maio
National Physical Laboratory (NPL), Hampton Road,
Teddington TW11 0LW, UK
e-mail: miguel.monclus@npl.co.uk

T. J. Young
The University of Surrey, Guildford, Surrey GU2 7XH, UK

Introduction

The most common technique used for the characterization of small volumes of material is instrumented indentation (IIT). The ultimate lateral resolution is limited by the applied force and the size of the indenter, which normally has a pyramidal (Berkovich) geometry with tip radius in the 150–300 nm range. IIT involves pressing the indenter tip into the surface of the sample whilst monitoring the force and displacement, and the calculation of the surface hardness and elastic modulus is usually carried out using the Oliver and Pharr method [1]. However, for certain applications such as composite interface characterization and thin layers, IIT does not necessarily have the required lateral resolution.

In advanced composite materials, it is now increasingly important to assess the quality of the interface between the reinforcement and the matrix, which facilitates improvements to composite predictive models [2]. In published literature [3–6], IIT or atomic force microscopy (AFM) are often used to characterize the interface region, in which, depending on the type of sizing applied to the reinforcement, interphase layers of varying thickness (1–5 μm) are expected; however, tests generally suffer from either lack of resolution (i.e. size of the probe in IIT) or surface artefacts (i.e. sharp probe interaction with surface features in AFM) and cannot probe the properties of the interphase region conclusively.

Another application that requires high lateral resolution methods is the study of intermetallic compounds (IMCs) of

1–2 μm thickness, which are usually formed between a solder alloy and a Cu metallic substrate. These IMCs (typically η-Cu_6Sn_5) grow during soldering, when the molten solder contacts the Cu substrate. The elastic modulus is a good indicator of the structural health of a solder joint subjected to thermal-fatigue [7]. The degradation of the elastic modulus can easily be measured in the solder alloy, and can be related to the number of micro-cracks developed in a thermal-fatigue test. However, this measurement cannot be done in IMC layers due to their very small thickness, and therefore, their mechanical degradation during fatigue is unknown. The Cu–solder joints can be mechanically characterized after annealing them, in order to increase the thickness of the IMC. This allows IIT to be carried out within the IMC region of interest [8–12], but annealing can alter the IMC microstructure [10, 11]. However, for real as-prepared IMCs of less than 2 μm in size IIT generally lacks the lateral resolution because the required indents are too large.

With AFM indentation, smaller tips (radius < 100 nm) can be used to indent the sample surface, and it is possible to produce arrays of low force indentations (force curves (FCs)) over the desired region with well-controlled position accuracy [13]; however, quantitative test methods based on AFM are complicated by surface preparation and a number of assumptions about the tip geometry and applied forces [14]. In the AFM indentation method proposed here, reference materials are used to estimate the tip radius and FCs are analysed to produce modulus maps across the region of interest. In this article, we report quantitative high-resolution measurements of the elastic modulus distribution around a glass flake-reinforced polymeric composite and a Cu–solder joint, which overcome the limited resolution of IIT. Elastic modulus values show good agreement with those obtained by IIT.

Materials and experimental details

The test method was carried out on two case studies: a Microglass® glass flake-reinforced polypropylene composite sample (GFRP) supplied by NGF Europe with 0.28 wt% aminosilane sizing applied to the glass flakes before processing and a solder (99Sn0.3Ag0.7Cu) joint on a Cu substrate sample. The surface preparation method used for the GRFP sample was a modified version of the mechanical polishing method employed by Khanna et al. [15] with an additional ultrasonic bath treatment. The Cu–solder joint was produced using a selective soldering method on an electrodeposited copper substrate. The joint was then cross-sectioned with a diamond saw and cold mounted in epoxy, ground, mechanically polished and finished with 0.4 μm colloidal silica to provide a smooth surface for cross-sectional IIT and AFM analysis. A sapphire sample was used to calibrate the compliance of the cantilever and an NPL CRM® fused silica and 18k Au samples, with reduce modulus (E_r) of 65.1 and 67.3 GPa, respectively, as measured by IIT, were used as reference materials. These materials were chosen because of their well-characterized elastic modulus and similar hardness to the glass flakes and the solder joint sample. All of the reference samples used had been polished to an rms roughness of <2 nm as measured from 10 × 10 μm^2 topography scans obtained by AFM.

A Park XE-100 AFM instrument was used in force volume mode for AFM indentation tests. A Micro Star Technology® TD13542 sapphire cantilever with a single crystal diamond tip with a sub 20 nm radius (as received) and a 7° cone angle was used. Micro Star Technology® employs a procedure to make a sapphire cantilever with a specified stiffness k (200 N/m in our case) where the beam is cut until the desired resonant frequency is achieved [16]. The stiffness of the AFM probe, in conjunction with the calibrated vertical movement of the piezo scanner, was used to infer the applied forces, which were in the range 3–5 μN. Scanning electron microscope (SEM) images of the tip after the AFM indentations reported here can be seen in Fig. 1. The AFM probe exhibited a small rate of change during indentations on the GFRP and reference samples, with a measured tip radius of less than 20 nm after the experiments as shown in Fig. 1a. It is worth noting the difficulty of accurate measurements of small tip radius because the quality of images is prone to vibrations and drift due to charging of the tip; the tip was rotated in the SEM in order to ensure that no asperities or imperfections were present and that the estimated radius is in fact a good approximation of the actual tip. The tip got damaged after further sets of indentations performed on different samples and was re-shaped by focused ion beam (FIB) before the next set of indentations for the Cu–solder joint sample. Figure 1b shows an SEM image of the AFM tip after re-shaping and after indentations on the Cu–solder and reference samples, with a final measured tip radius of

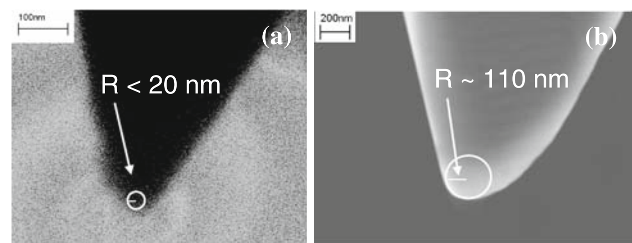

Fig. 1 SEM images of the diamond tip used for AFM indentation experiments: **a** tip after AFM indentations set on the GFRP and reference samples; **b** indenter tip after re-shaping with FIB and indentations set on the Cu–solder joint and reference samples

~110 nm. SEM images in Fig. 1a and b are oriented with the cantilever in a horizontal position. As the engagement angle of the probe on the sample surface with respect to a horizontal plane is ~12°, the actual values for the contact radii approximate the ones estimated from the images.

The AFM indenter tip is mounted at the end of a cantilever beam and a piezoelectric actuator controls the displacement towards the surface. For each indentation, the cantilever is brought towards the surface along the *Z*-axis and the deflection of the cantilever is measured by a laser reflecting off the back of the cantilever using a position-sensitive photo-diode, which gives an output voltage signal. The raw-measured indentation data are, therefore, a cantilever deflection voltage versus the distance the cantilever has moved towards the surface. The voltage axis is then converted to cantilever deflection by using a sensitivity factor obtained from the slope of a linear fit to the contact portion of the voltage–distance curve obtained on the hard sapphire sample (assuming that all measured deflection is due to bending of the cantilever and there is no indentation of the surface). The cantilever deflection (d) is finally converted to force, F, using $F = d \times k$ (assuming calibrated cantilever spring constant, k).

For each raw FC obtained on the reference and test samples, the analysis software (written in MATLAB®) selects the zero point for penetration distance from the approach curve as the first set of a predefined number of points, which lie above the constant voltage measured during approach by a predefined threshold (typically set to 0.1%). The analysis software then discards the portion of the data representing the non-contact region.

The next step in the analysis software is to subtract the cantilever response on the sapphire sample (by assuming a non-penetrating contact) from the total measured cantilever deflection on the reference and test samples in order to generate a more accurate indentation distance for each curve. This is depicted in Fig. 2, where an example is given

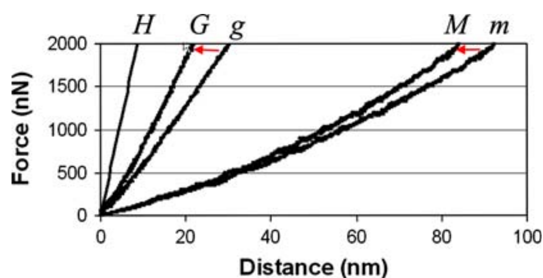

Fig. 2 Force versus distance plots showing how the loading FC on the hard reference sample (*H*) is subtracted from the loading FC on the glass fibre and polymer matrix (*g* and *m*) to produce the corrected loading FCs (*G* and *M*)

of indentation 'loading' FCs being corrected for indents on the glass and polymer matrix materials.

The corrected indentation loading curves were fitted with the general Sneddon's expression for the force–displacement relationship [17], given in Eq. 1, where F is the applied force, h the indentation depth, n equals 1.5 for a spherical contact and α an unknown constant, which is calculated from the power-law fit. AFM indentation arrays (4×4 indents, spacing = 0.5 μm) performed on reference samples before and after the test sample were used to estimate the unknown tip radius (R) from the average value of the 16 indents, and also to check for tip shape stability. For the Hertzian model considered here [18], the tip radius R was calculated using Eq. 2, where $E_{r(ref)}$ is the reduced modulus of the reference sample:

$$F = \alpha h^n, \quad (1)$$

$$R = \left(\frac{3\alpha}{4E_{r(ref)}} \right)^2. \quad (2)$$

The reduced elastic modulus for the 'unknown' sample, E_r, was then calculated for each indent of the indentation array selected to test the sample using:

$$E_r = \frac{3\alpha}{4\sqrt{R}}, \quad (3)$$

and finally, the Young's elastic modulus of the sample, E_s, was obtained using Eq. 4, which takes into account the diamond tip elastic deformation, where the subscript s and I denote sample and tip, respectively, υ the Poisson's ratio and E the elastic modulus:

$$\frac{1}{E_r} = \frac{(1 - \upsilon_s^2)}{E_s} + \frac{(1 - \upsilon_I^2)}{E_I}. \quad (4)$$

AFM amplitude images of the GFRP sample were obtained using a Si tip (stiffness $k \sim 2.8$ N/m) with the sample vibrated by an Olympus NDT ultrasonic transducer (2.25 MHz central frequency) at a frequency of ~305 kHz, close to the frequency of the cantilever flexural resonance when in contact with the sample surface [19]. IIT experiments were performed using an MTS Nano Indenter® instrument fitted with a Berkovich diamond tip with a 250 nm end radius as estimated by AFM. Quasi-static indentations were made using constant loading and unloading times of ~30 s, and a hold period at maximum constant force of 60 s to minimize creep effects. The maximum indentation force used was 1 mN for the Cu–solder joint and reference samples, whereas for the GFRP sample, the maximum forces used were 0.5 and 2 mN. For the GFRP sample, the indenter instrument was also used in continuous stiffness mode, which is more suited for materials exhibiting viscoelastic behaviour [20]; for these experiments, the oscillation frequency was set to 40 Hz with a constant force amplitude of 3 μN.

Results and discussion

Glass flake-reinforced polypropylene sample (GFRP)

Figure 3a shows an optical image of the GFRP sample surface, where embedded glass flakes of random size, geometry and dispersion can be observed. AFM topographical and amplitude images of an interface region (4×4 μm^2 scan size) taken simultaneously are shown in Fig. 3b. By measuring the AFM cantilever amplitude, variations of the contact stiffness between tip and sample surface are highlighted; the choice of the operating frequency causes exposition of contrasting features [18]. In this case, the stiffer region (glass) appears brighter than the softer region (polymer), and there is an abrupt boundary between the two regions.

An array of 58×12 indentations covering a 4×0.8 μm^2 region was performed over the glass–matrix interface. The separation between indents (~69 nm) should be sufficiently small to detect any possible extended interface region with distinct mechanical properties. The very low applied forces (<3 μN) also minimized the possibility of plastic deformation and overlapping of indents. Typical loading curves for the glass and polymeric matrix are presented in Fig. 4. The analysis assumes that only elastic deformation occurs during loading. Whether Hertz conditions can be met in an AFM nanoindentation experiment will depend on the material under consideration and the stress applied by the probe, which is determined by the stiffness of the cantilever and the probe geometry. Due to the very low forces applied here, typically, no hysteresis between loading and unloading curves, and no indication of residual indents are observed in post-indentation AFM scans, indicating purely elastic deformation, despite the relatively stiff cantilever ($k \sim 200$ N/m) and sharp tip probe (radius < 20 nm) used for these experiments. Figure 5 shows four lines of the measured reduced modulus across the glass–matrix interface, and the inset in Fig. 5 presents the reduced modulus map across the whole 4×0.8 μm^2 region of the interface region. No measurable interface region with different elastic properties to the glass and the matrix can be detected, in agreement with the AFM amplitude image in Fig. 3b.

In some measurements (not shown here) taken on different sites across the interface, a few intermediate points with modulus values between the glass and the matrix can be observed. As the tip indents closer to the fibre, uneven loading beneath the tip causes the tip to indent more on the softer more compliant material, producing a twist of the AFM probe. In addition, surface features such as a step or a wedge at the interface can cause the AFM probe to twist. These measurement artefacts can be detected by monitoring the lateral force, and the latest results, which are currently under investigation, show that the intermediate values measured at the interface are due to measurement artefacts, rather than a real interface material property.

The averaged measured reduced elastic modulus and standard deviation values for the polypropylene matrix and glass flake are 4.1 ± 0.9 and 63.5 ± 4.1 GPa, respectively. Young's modulus values (E_s) of 3.4 and 65.5 GPa can be calculated with Eq. 4, using the properties of the diamond indenter tip ($v_I = 0.07$ and $E_I = 1{,}140$ GPa) and v_s values for the matrix and glass of 0.42 and 0.16, respectively. The polypropylene modulus of 3.4 GPa found here is higher than the bulk modulus value of 1.9 GPa determined from tensile testing given by the manufacturer. Polymeric materials create significant challenges to measuring modulus accurately using indentation testing [19]. The tip radius estimated from the fused silica reference material is not accurate enough for calculations of the matrix modulus due to the difference in hardness between fused silica and

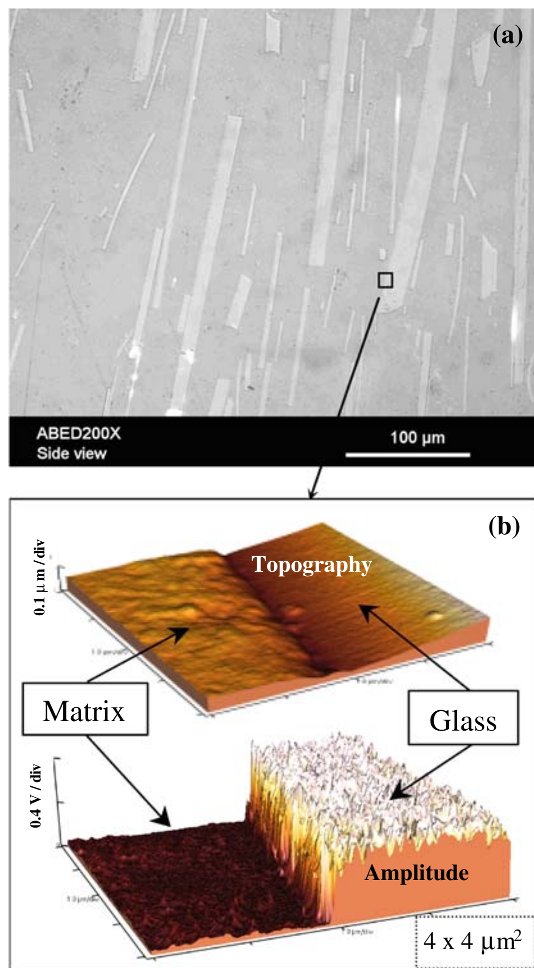

Fig. 3 **a** Optical image of the glass flake-reinforced polypropylene; **b** 4×4 μm^2 AFM topographical image taken in contact mode (*top*) and 4×4 μm^2 AFM amplitude image (*bottom*) of the interface region

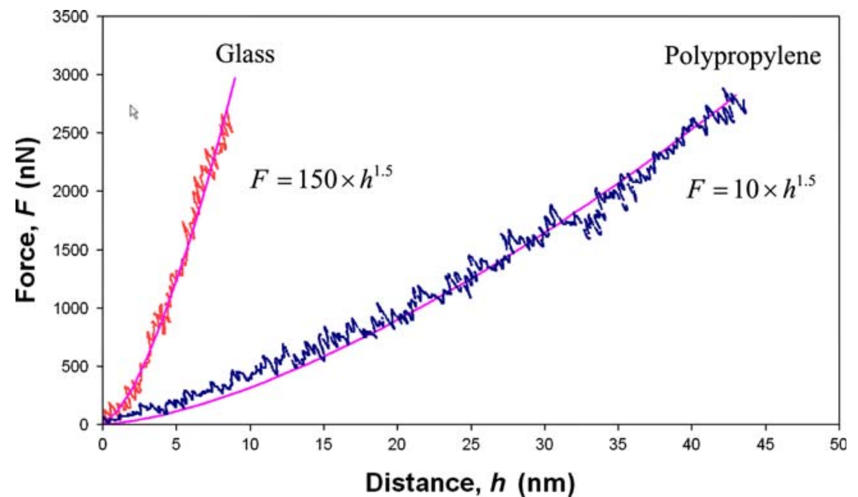

Fig. 4 Typical force–distance loading curves corresponding to indent locations on the glass flake (*left*) and polypropylene matrix (*right*), showing the applied Hertzian fit equations

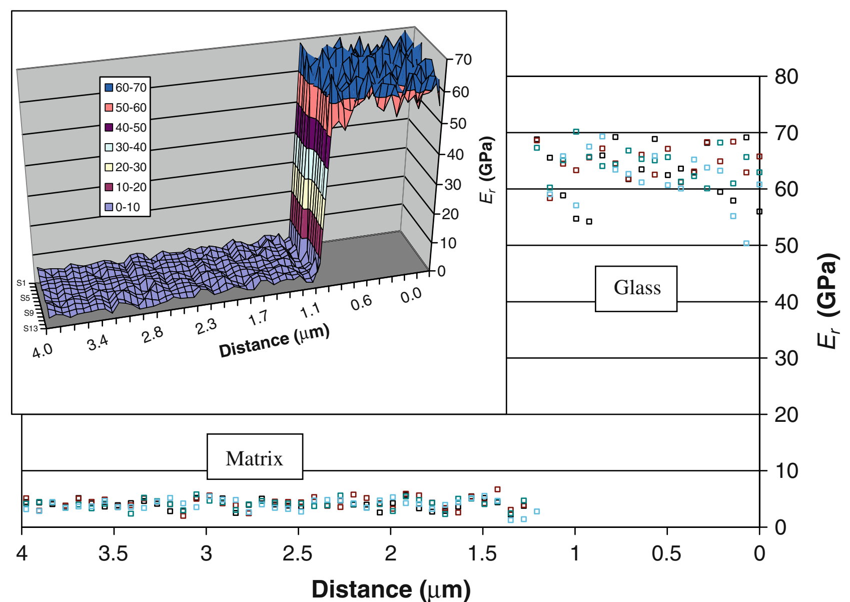

Fig. 5 Reduced elastic modulus values obtained over the interface of the GFRP sample across four lines of indents of 4 μm in length and 69 nm separation between them. The *inset* shows the reduced elastic modulus values mapped over the whole 4 × 0.8 μm^2 interface region obtained from the applied 58 × 12 indentation matrix

polypropylene; when pushing the probe into the polymer, contact depths are beyond those achieved on fused silica, and therefore, extrapolation of the tip radius deduced from fused silica measurements becomes error prone; as a result calculations of the modulus of a polymeric matrix when indenting with a non-ideal spherical tip apex will tend to overestimate the modulus, since the actual contact radius would be larger than the estimated value.

Instrumented indentation testing was carried out on the GFRP sample. Figure 6 shows typical force–displacement curves obtained for 2 mN maximum depth and an optical image indicating where the indentations were performed. Modulus values for the glass material were obtained using the Oliver and Pharr method from selected indents located in the middle of the flakes, whereas for the matrix, modulus values were calculated using the continuous stiffness method from indents located at least 5 μm away from the glass flakes edges.

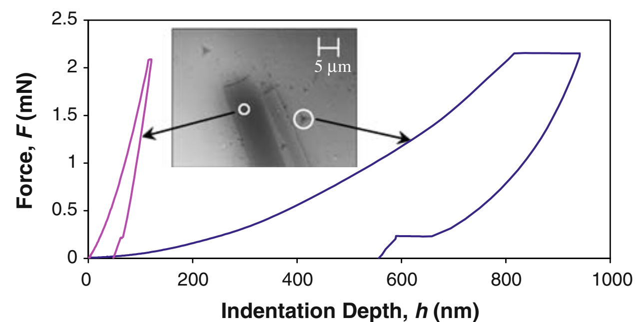

Fig. 6 IIT force–displacement curves obtained for the glass flake and polypropylene matrix; the *inset* shows an optical image of the indentation site where the locations of the indents corresponding to each force–displacement curve are *circled*

Average IIT Young's modulus values and standard deviations for five indents on the glass flake and polypropylene matrix materials are shown in Table 1, where they

Table 1 Young's modulus (E_s) values for the glass flake and the polypropylene matrix for the GFRP sample calculated from instrumented indentation (IIT) and the AFM indentation method described in this work (uncertainties are one standard deviation of the mean)

Material	IIT E_s (GPa)	AFM E_s (GPa)
Glass flake	61.0 ± 0.2	65.5 ± 4.8
Polypropylene	2.5 ± 0.1	3.4 ± 0.9

are compared with those obtained by the AFM indentation method. Good agreement was found for the glass flake, whereas there is bigger discrepancy for the polypropylene values, due to the spherical tip shape assumption made to analyse the AFM data.

Cu–solder joint sample

Figure 7a shows an SEM image of the Cu–solder(Sn) region, where an IMC layer of varying thickness (1–2 μm) can be distinguished. Energy dispersive X-ray (EDX) compositional analysis was made across this IMC layer as shown in Fig. 7b. The atomic compositional analysis shows that the associated IMC layer is mainly Cu_6Sn_5 with a thickness varying from 1 to 2 μm.

The described AFM indentation method, using the gold sample as reference material, was applied to the Cu–solder joint sample. For the array of indentations performed here, a minimum separation of ~470 nm was found necessary to avoid adjacent indents affecting each other. Figure 8a shows a 15 × 15 μm^2 AFM scan image taken in contact mode where two 32 × 4 indentation arrays (covering a 15 × 2 μm^2 area each) were performed over the interface. In the AFM scan, residual indents on the softer Sn side can be clearly seen, which indicates that the deformation has gone partially plastic, but little or no hysteresis is observed between loading and unloading curves, indicating mainly elastic deformation. The relatively large hemi-sphere radius of the used tip reduces the possibility of exceeding the elastic limit of the material under analysis. The very low applied forces (<5 μN) also minimized the possibility of plastic deformation and overlapping of indents. Typical loading curves for the IMC, Cu and solder materials are shown in Fig. 8b, where different penetration distances for the same maximum force are observed for the three types of material. The curves were fitted with a Hertzian power-law as described in 'Materials and experimental details' section. The reduced modulus calculated from one set of indentation arrays is shown in Fig. 8c as a line plot, where a noticeably separate IMC layer of higher modulus can be clearly observed, of up to 2 μm in thickness. The average values for the reduced modulus of the Cu, solder and IMC regions were 56.3 ± 2.1, 76.9 ± 0.8 and 130.3 ± 5.6 GPa, respectively. The observed scatter in the data is mainly due to variations in sample roughness across the investigated region (R_a is ~5 nm across a 10 × 10 μm^2 region), which is approximately 17% of typical indenter penetration depths (~30 nm). Reduced modulus values were converted to Young's modulus with Eq. 4 using literature [6] Poisson's ratio (ν_s) values for Sn (0.4), Cu (0.36) and Cu_6Sn_5 (0.33).

Instrumented indentation testing on the Cu–solder joint sample was performed next, with lines of indents 5 μm apart made at small angles to the IMC layer in order to maximize the chance of hitting the IMC layer, as shown in Fig. 9a, where the darker IMC layer of ~1 μm can be distinguished. It should be noted that IIT testing using a separations of 50 μm between indents across the Cu and solder regions was performed in order to make sure that the values obtained with 5 μm indent separation were not affected by plastic zone overlapping [20]. The force–displacement curves corresponding to solder, Cu and IMC regions are shown in Fig. 9b. The solder was found to be very soft, with a hardness of 0.19 ± 0.02 GPa and exhibiting significant plasticity. The measured hardness for the Cu and IMC were 1.54 ± 0.1 and 3.0 ± 1.3 GPa, respectively. IIT Young's modulus for the solder, Cu and IMC materials were 46.4 ± 4.8, 73.5 ± 3.4 and 89.4 ± 9.1 GPa, respectively. For the Cu and solder, the values represent an average of eight indentations and the uncertainty given is the standard deviation of the mean. The IMC

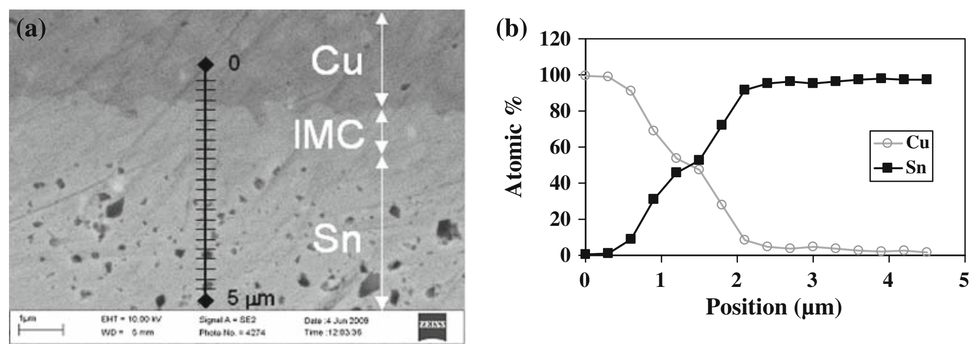

Fig. 7 **a** Cross-sectional SEM image of the Cu–solder(Sn) interface region showing a 5-μm line where the EDX analysis was performed; **b** EDX atomic concentration profile across the interface region, showing an IMC layer of up to 2 μm in thickness

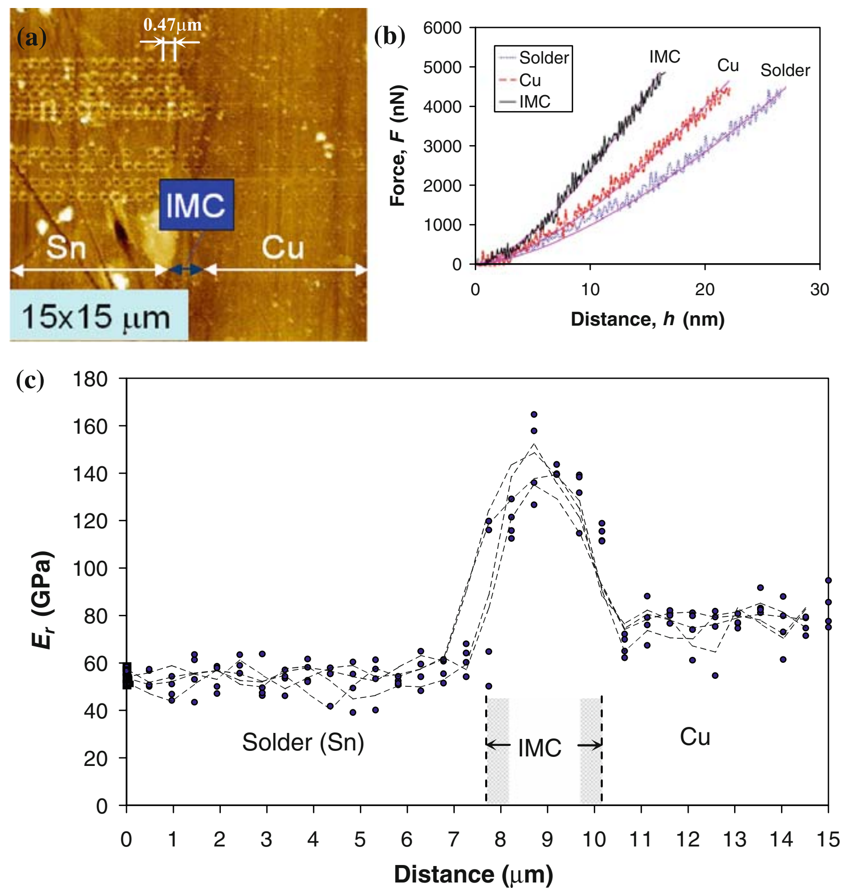

Fig. 8 **a** 15 × 15 µm AFM scan image showing the approximate position of the IMC layer; the location of two 32 × 4 indentation arrays can be identified; **b** force–distance loading curves corresponding to indent locations on the IMC, Cu and solder materials, showing the applied Hertzian fit; **c** moving average of reduced modulus values corresponding to four lines of 32 AFM indentations across a 15 × 2 µm^2 region separated by 0.47 µm

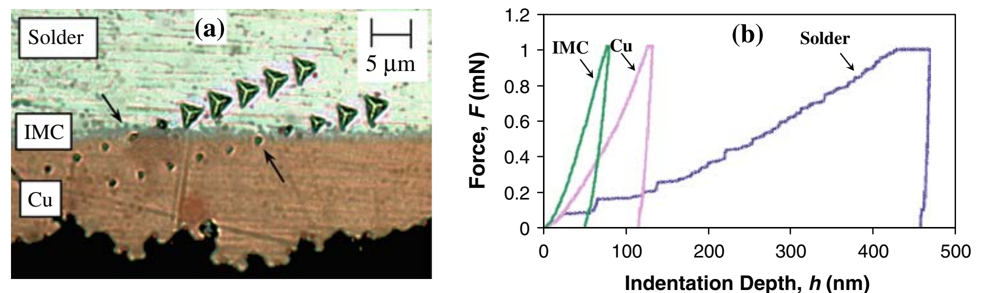

Fig. 9 **a** Optical image showing the location of the indents across the Cu–solder interface; the *arrows* indicate the two indents closer to the centre of the darker IMC layer ~1 m thick; **b** IIT force–displacement curves for the solder, Cu and IMC materials

hardness and elastic modulus values are an average of just two values obtained at the specific indent locations indicated by arrows in Fig. 9a. The Young's modulus calculated for the three materials are summarized in Table 2, where they are compared with those obtained by the AFM indentation method. AFM indentation values for Cu and Sn are very close to those measured by IIT despite the assumption of linearly elastic AFM indentations with negligible adhesion interactions. There is a much bigger discrepancy for the IMC layer modulus values. The value of 89.4 GPa obtained by IIT is not representative of the IMC layer, because it is very difficult to ensure that only the IMC material is being tested due to the larger size of the indenter and the relatively large applied forces.

Table 2 Young's modulus (E_s) values for the solder, Cu and IMC regions of the Cu–solder joint sample calculated from instrumented indentation (IIT) and the AFM indentation method described in this work (uncertainties are one standard deviation of the mean)

Material	IIT E_s (GPa)	AFM E_s (GPa)
Solder (Sn)	46.4 ± 4.8	49.8 ± 2.1
Cu	73.5 ± 3.4	71.8 ± 0.8
IMC	89.4 ± 9.1	131.1 ± 5.6

However, the AFM indentation value of 131.1 GPa obtained with the present method was obtained at much lower forces and with a smaller tip, and the value agrees well with those expected for this type of IMC layer [12].

Concluding remarks

We have successfully applied an AFM indentation test method to map the elastic modulus around a composite interface and a Cu–solder joint. An algorithm for analysing multiple AFM indentation curves has been tested and true nanoscale spatial resolution was achieved through the use of low applied forces (<3 μN) and a sharp AFM diamond tip. The applied method assumes Hertzian contact and relies on the use of reference materials to estimate the tip radius and making sure the tip has not been damaged during experimentation.

The AFM indentation method applied over the interface of a GFRP composite indicates the absence of a distinct interface layer with different elastic properties. This is in agreement with AFM amplitude images of the interface, which do not indicate the presence of a separate layer of different stiffness. The measured elastic modulus for the glass flake agrees well with IIT testing, while the obtained elastic modulus value for the polymeric matrix differ by $\sim$30% due to inaccurate radius tip estimation using the harder fused silica reference sample, which leads to an overestimation of the elastic modulus. The applied method over a Cu–solder joint detected an IMC layer (1–2 μm thick) with much higher modulus value than Cu and solder, in agreement with the value expected for this type of IMC. The elastic modulus values obtained for the Cu and solder material also show an excellent agreement with those obtained from IIT testing.

The main advantage of the proposed AFM method is the ability to produce high-resolution maps of elastic modulus, which, coupled with the higher position accuracy of AFM instruments, offers an advanced measurement tool for applications where conventional indentation testing lacks the required lateral resolution.

Acknowledgements The authors gratefully acknowledge funding from the UK Government Department of Business, Innovation and Skills.

References

1. Oliver WC, Pharr GM (1992) J Mater Res 7(6):1564
2. Broughton WR, Crocker LE, Loderio MJ (2006) NPL Report DEPC-MPR 055
3. Hodizc A, Stachurski ZH, Kim JK (2000) Polymers 41:6895
4. Hodizc A, Kim JK, Stachurski ZH (2001) Polymers 42:5701
5. VanLandingham MR, Dagastine RR, Eduljee RF, McCullough RL, Gillespie JR (1999) Composites A 30:75
6. Kim JK, Sham ML, Wu J (2001) Composites A 32:607
7. Budiansky B, O'Connel RJ (1976) Int J Solids Struct 12(2):81
8. Li D, Liu C, Conway PP (2005) Mater Sci Eng A 391:95
9. Jang GY, Lee JW, Duh JG (2004) J Electron Mater 33(10):1103
10. Chromik RR, Vinci RP, Allen SL, Notis MR (2003) J Mater 55(6):66
11. Yang PF, Lai YS, Jian SR, Chen J, Chen RS (2008) Mater Sci Eng A 458:305
12. Chromik RR, Vinci RP, Allen SL, Notis MR (2003) J Mater Res 18(9):2251
13. Lin DC, Dimitriadis EK, Horkay F (2007) Trans ASME 129(3):430
14. Butt HJ, Capella B, Kappl M (2005) Surf Sci Rep 59:1
15. Khanna SK, Winter RM, Ranganathan P, Yedla SB, Kalukanimuttam M, Paruchuri K (2003) Composites A 34(1):53
16. Mesa B, Magonov S (2007) J Phys Conf Ser 61:770
17. Sneddon IN (1965) Int J Eng Sci 3(1):47
18. Johnson KL (1985) Contact mechanics. Cambridge University Press, Cambridge
19. Rabe U, Amelio S, Kester E, Scherer V, Hirsekorn S, Arnold W (2000) Ultrasonics 38:430
20. Oliver WC, Pharr GM (2004) J Mater Res 19(1):13